Available online at www.sciencedirect.com

SciVerse ScienceDirect

Geochimica et Cosmochimica Acta 75 (2011) 6556–6569

Geochimica et Cosmochimica Acta

www.elsevier.com/locate/gca

Petrology and oxygen isotope compositions of chondrules in E3 chondrites

Michael K. Weisberg [a,b,c,*], Denton S. Ebel [b,c], Harold C. Connolly Jr. [a,b,c], Noriko T. Kita [d], Takayuki Ushikubo [d]

[a] Department of Physical Sciences, Kingsborough College, City University of New York, Brooklyn, NY 11235, United States
[b] Department of Earth and Environmental Sciences, Graduate Center of City University of New York, New York, NY 10016, United States
[c] Department of Earth and Planetary Sciences, American Museum of Natural History, New York, NY 10024, United States
[d] WiscSIMS, Department of Geoscience, University of Wisconsin-Madison, WI 53706, United States

Received 1 March 2011; accepted in revised form 29 August 2011

Abstract

Chondrules in E3 chondrites differ from those in other chondrite groups. Many contain near-pure endmember enstatite ($Fs_{<1}$). Some contain Si-bearing FeNi metal, Cr-bearing troilite, and, in some cases Mg, Mn- and Ca-sulfides. Olivine and more FeO-rich pyroxene grains are present but much less common than in ordinary or carbonaceous chondrite chondrules. In some cases, the FeO-rich grains contain dusty inclusions of metal. The oxygen three-isotope ratios ($\delta^{18}O$, $\delta^{17}O$) of olivine and pyroxene in chondrules from E3 chondrites, which are measured using a multi-collection SIMS, show a wide range of values. Most enstatite data plots on the terrestrial fractionation (TF) line near whole rock values and some plot near the ordinary chondrite region on the 3-isotope diagram. Pyroxene with higher FeO contents (~2–10 wt.% FeO) generally plots on the TF line similar to enstatite, suggesting it formed locally in the EC (enstatite chondrite) region and that oxidation/reduction conditions varied within the E3 chondrite chondrule-forming region. Olivine shows a wide range of correlated $\delta^{18}O$ and $\delta^{17}O$ values and data from two olivine-bearing chondrules form a slope ~1 mixing line, which is approximately parallel to but distinct from the CCAM (carbonaceous chondrite anhydrous mixing) line. We refer to this as the ECM (enstatite chondrite mixing) line but it also may coincide with a line defined by chondrules from Acfer 094 referred to as the PCM (Primitive Chondrite Mineral) line (Ushikubo et al., 2011). The range of O isotope compositions and mixing behavior in E3 chondrules is similar to that in O and C chondrite groups, indicating similar chondrule-forming processes, solid–gas mixing and possibly similar ^{16}O-rich precursors solids. However, E3 chondrules formed in a distinct oxygen reservoir.

Internal oxygen isotope heterogeneity was found among minerals from some of the chondrules in E3 chondrites suggesting incomplete melting of the chondrules, survival of minerals from previous generations of chondrules, and chondrule recycling. Olivine, possibly a relict grain, in one chondrule has an R chondrite-like oxygen isotope composition and may indicate limited mixing of materials from other reservoirs. Calcium–aluminum-rich inclusions (CAIs) in E3 chondrites have petrologic characteristics and oxygen isotope ratios similar to those in other chondrite groups. However, chondrules from E3 chondrites differ markedly from those in other chondrite groups. From this we conclude that chondrule formation was a local event but CAIs may have all formed in one distinct place and time and were later redistributed to the various chondrule-forming and parent body accretion regions. This also implies that transport mechanisms were less active at the time of and following chondrule formation.

* Corresponding author at: Department of Physical Sciences, Kingsborough College, City University of New York, Brooklyn, NY 11235, United States.
E-mail address: mweisberg@kbcc.cuny.edu (M.K. Weisberg).

0016-7037/$ - see front matter © 2011 Elsevier Ltd. All rights reserved.
doi:10.1016/j.gca.2011.08.040

1. INTRODUCTION

Enstatite (E) chondrites are records of highly reducing conditions in the early solar system (e.g., Keil, 1968). The major silicate phase is enstatite (FeO < 1.0%). They contain high amounts of FeNi metal and it is Si-bearing, with more than 2 wt.% Si in EH metal. The EH chondrites also contain perryite (Fe–Ni silicide), as well as Mg-, Mn-, and Ca-bearing sulfides, the oxi-nitride sinoite (Si_2N_2O) (Andersen et al., 1964; Keil and Andersen, 1964; Mason, 1966; Keil, 1968) and the nitride phase osbornite (TiN) (Mason, 1966). All of these minerals are indicators of highly reducing conditions. The Hvittis EL6 was shown to have a remarkably low intrinsic fO_2 compared to other chondrites (Brett and Sato, 1984). In spite of their remarkable characteristics, the chondrules in enstatite chondrites have received considerably less attention than chondrules in other groups and their origin and relationship to chondrites in other groups are unclear.

Another intriguing characteristic of the enstatite chondrites is that they are the only chondrites with whole rock oxygen isotopic compositions that are similar to the Earth and Moon (Clayton and Mayeda, 1984; Javoy, 1995). However, prior to this work, little was known about the range of oxygen isotopic compositions of individual chondrules in the E3 chondrites. Here we present the results of our detailed petrologic and oxygen isotope study of olivine and pyroxene in chondrules from three E3 chondrites: Sahara 97096 and Yamato 691 (Y 691), both EH3, and Lewis Cliff 87223 (LEW 87223), an anomalous E3. Our goals are to (1) document the mineral compositions and oxygen isotope ratios of olivine and pyroxene in the E3 chondrules, (2) explore the relationship between enstatite, the dominant mineral in E3's, and the less common olivine and FeO-rich low-Ca pyroxene and (3) shed light on the origin of chondrules in E3 chondrites and their relationship to chondrules in chondrites of other groups. Note that the term "FeO-rich" is used here to refer to grains in E3 chondrites having >2 wt.% FeO. These grains are in contrast to the more common enstatite which typically has less than 2 wt.% FeO.

2. METHODS

Sahara 97096 and Y 691 were selected because they are among the most primitive EH3 chondrites (Weisberg et al., 2005). LEW 87223 was selected because it contains a high abundance of FeO-rich pyroxene, generally rare in E3 chondrites and essentially absent in equilibrated E chondrites. Thin sections of Sahara 97096 (AMNH 4940-1), Yamato 691 (AMNH 4952-1) and LEW 87223,11 were documented with transmitted light photomicrographs and backscattered electron (BSE) images using the JEOL JSM-6390 scanning electron microscope with Bruker Quantax EDS and Hitachi S4700 Field Emission Gun Scanning Electron Microscope (FEG-SEM), equipped with a PGT EDS. Chondrules with a wide range of texture, composition and mineral assemblage were selected using these instruments. Maps of Si, Al, Mg, Ca, Fe and Ni X-ray emission intensity in the entire section were generated with the Cameca SX100 electron microprobe. These are "stage maps" (moving stage, stationary electron beam). Operating conditions were 15 kV and 40 nA, with a dwell time of 12 ms on one micrometer beam spots spaced 7 μm apart on each of 36 512 × 512 pixel maps. Composite X-rays of the thin sections are displayed in Fig. 1. These maps were used to further select chondrules having high amounts of olivine and or FeO-rich pyroxene.

Mineral compositions were determined using the Cameca SX100 electron microprobe at the American Museum of Natural History. Natural and synthetic standards were chosen based on the compositions of the minerals being analyzed. An accelerating potential of 15 keV and a sample current of 20 nA were used for silicate and 20 keV and 25 nA for metal. Counting times were 20 s on peak, and 10 s on background (off-peak) spectrometer positions. Relative uncertainties (2σ), based on counting statistics, for major elements (Si, Fe, Mg) are calculated to be <2% and for Ti, Cr, Mn and Ca they are 10%, 10%, 9% and 5%, respectively. Data reductions were carried out using methods described by Pouchou and Pichoir (1991).

The ion microprobe CAMECA IMS-1280 at the University of Wisconsin-Madison (WiscSIMS, Kita et al., 2009) was used for the oxygen three-isotope analyses of olivine and pyroxene, the dominant minerals in the chondrules studied. The analytical procedure is very similar to that described in Kita et al. (2010) using three Faraday cups on the multi-collection system for high precision oxygen three isotope analyses. We used a Cs^+ primary beam of ~4 nA focused to a 15 μm diameter and obtained secondary ^{16}O intensities at $\sim 3 \times 10^9$ count per seconds (cps), which corresponds to ^{17}O intensities at $\sim 1 \times 10^6$. A single analysis took ~7 min per spot. Typically ~15 unknown analyses of olivine and low-Ca pyroxene in chondrules are bracketed by a total of eight analyses of the San Carlos olivine standard (Fo_{89}, $\delta^{18}O = 5.32‰_{VSMOW}$; Kita et al., 2010) that was mounted as a polished thin section. The average external reproducibilities of bracketing standard analyses (2SD) were 0.3‰ for $\delta^{18}O$ and 0.5‰ for $\delta^{17}O$ and $\Delta^{17}O$ during the session. Enstatite standard SP79-11 (En_{97} $\delta^{18}O = 13.31‰_{VSMOW}$; Kita et al., 2010) was analyzed in the same session to evaluate matrix effect between olivine and pyroxene (Kita et al., 2010). The instrumental bias of low-Ca pyroxene was −1.06‰ relative to the olivine standard, which was applied to the final data.

3. RESULTS

3.1. Texture

Properties of chondrules in E3 chondrites have been described previously (e.g., Leitch and Smith, 1982; Rambaldi et al., 1983; Grossman et al., 1985; Ikeda 1988, 1989; Weisberg et al., 1994; Schneider et al., 2002; Kimura et al., 2003), and Kimura et al. (2003) previously reported limited oxygen isotope ratios of FeO-rich silicates in E3 chondrites. Here we present petrologic data from nine chondrules and fragments in Sahara 97096, eight in Y 691 (both EH3) and five from the LEW 87223, an E3-annomalous chondrite (Fig. 1).

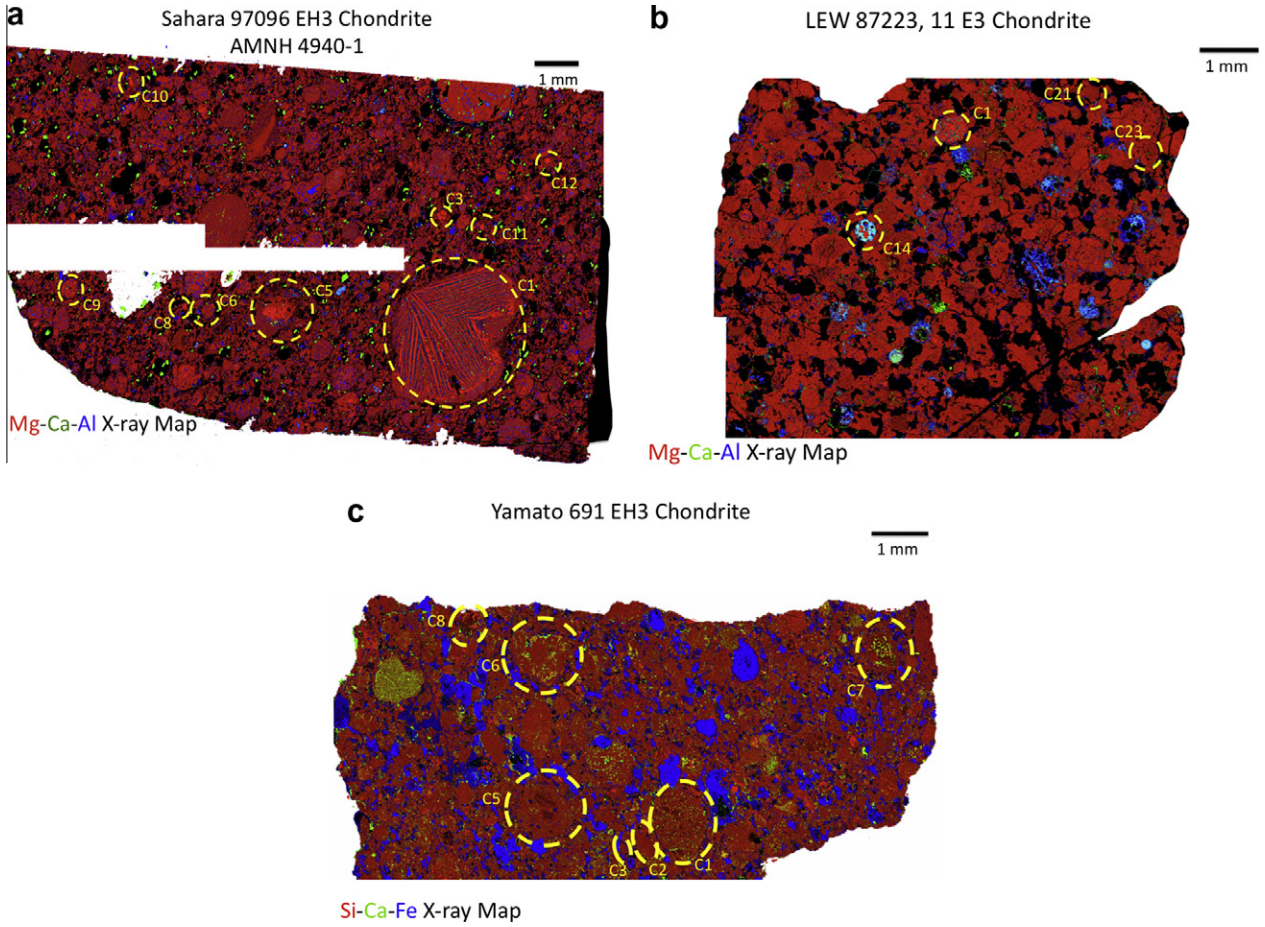

Fig. 1. Composite (red–green–blue) X-ray maps of polished thin sections of (a) Sahara 97096 (Mg–Ca–Al map), (b) LEW 87223 (Mg–Ca–Al map) and (c) Y 691 (Si–Ca–Fe map). The X-ray maps show the chondrules selected for study (circled by dashed lines), as well as the distribution of olivine in these meteorites. In 1a and 1b olivine is the bright red phase and in 1c it appears as the dullest red phase. Also note the higher abundance of Al-rich chondrules (with abundant blue-green mesostasis) in LEW 87223, specifically C14 which was analyzed in this study.

The chondrules studied are generally 500 μm–1 mm in diameter with one exception, a >3 mm barred olivine chondrule (Fig. 1a). Textures include porphyritic pyroxene (PP), porphyritic olivine–pyroxene (POP), porphyritic olivine (PO), a rare unusually large (>3 mm) barred olivine (BO), and an Al-rich chondrule (Figs. 1 and 2). Chondrules containing olivine in particular were selected to determine the relationship of olivine to enstatite. The porphyritic chondrules consist of low-Ca pyroxene (generally enstatite) ± olivine (generally absent in most E3 chondrules) with albitic glass ± silica and opaque minerals along cracks and as isolated blebs (Fig. 2a and b). Olivine-rich porphyritic chondrules (e.g., Fig. 2b) are very similar in texture to the type IA chondrules that are characteristic of O (ordinary) and C (carbonaceous) chondrites. However, some type I chondrules in EH3 chondrites contain silica (e.g., Fig. 2c), which is not common in type I chondrules in ordinary or carbonaceous chondrites. Additionally, Cr-bearing troilite is present in some chondrules. Although troilite may occur in type I chondrules in other chondrites, the Cr content is generally below electron probe detection limits. In a few EH3 chondrules, nodules with assemblages of troilite, Si-bearing metal ± oldhamite (CaS) ± niningerite (Mg,Fe,Mn)S are present.

Olivine occurs in different textural settings in chondrules. It occurs as bars in barred olivine chondrules that are texturally similar to some type I barred olivine chondrules in O and C chondrites (Fig. 1). In some chondrules, olivine occurs as poikilitic inclusions in enstatite (Fig. 2a). In one notable chondrule (Sah 97096 C11) olivine is present as large crystals (up to 200 μm) surrounded by fine enstatite and albitic glass and silica (Fig. 2c and d). The large olivine crystal in C11 is clearly not in textural equilibrium with the surrounding finer-grained assemblage of pyroxene and silica in this chondrule.

Of the chondrules studied, two from LEW 87223 (C21 and C23; Fig. 2g) contain FeO-rich pyroxene. Additionally, we studied a fragment from Sahara 97096 (C2, Fig. 2f) consisting of FeO-rich pyroxene, silica and it appears to be associated with enstatite. LEW 87223 C23 is particularly unusual and was reported previously by Weisberg et al. (1994). In C23, enstatite occurs both in the central region of the chondrule and on the edges and there is a vein of enstatite that extends from the edge to the center. This

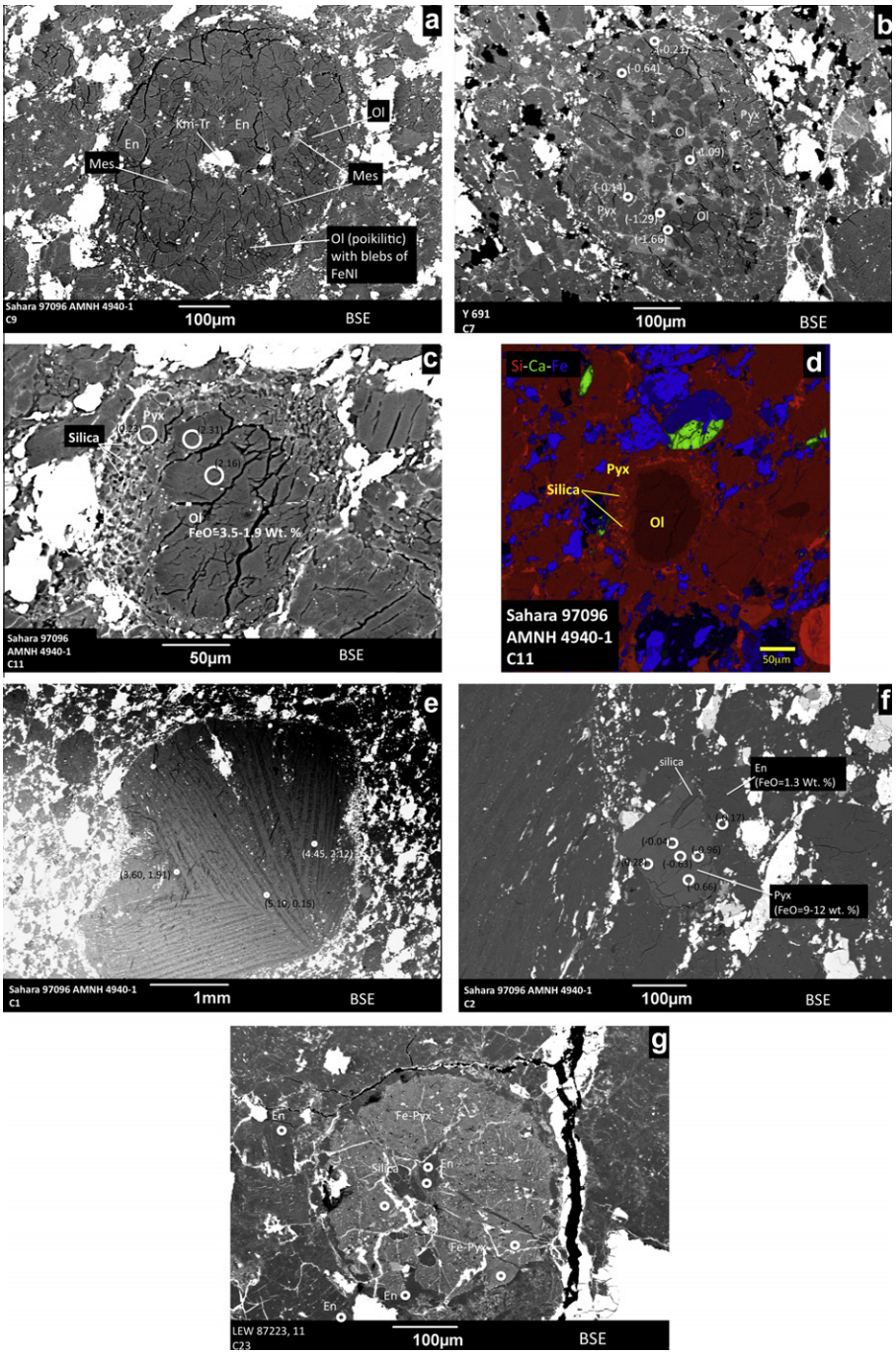

Fig. 2. BSE images and X-ray maps of chondrules from the enstatite chondrites studied. White circles on images show the areas in which oxygen isotopes were analyzed by SIMS. (a) Enstatite-rich chondrule C9 from Sahara 97096 composed of enstatite (En) with poikilitic olivine (Ol), a small amount of faldspathic mesostasis (Mes) and a kamacite-troilite nodule (km-Tr). (b) Porphyritic olivine pyroxene chondrule C7 from Y 691 composed of olivine (~15 µm) grains with an interstitial feldspathic mesostasis and coarser enstatite near the outer portion of the chondrule. Some enstatite contains poikilitic olivine. Numbers in parentheses are $\Delta^{17}O$ values for each spot analyzed. (c) Chondrule C11 from Sahara 97096 consisting of large olivine crystals (up to 200 µm) surrounded by finer enstatite and albitic glass and silica. (d) Si–Ca–Fe (red–green–blue) composite X-ray map of C11 showing the large olivine (dullest red) and the surrounding mixture of enstatite and silica (brightest red). (e) Barred olivine (BO) chondrule C1. BO chondrules are rare in E3 chondrites. C1 is over 4 mm across. Numbers in parentheses are $\delta^{18}O$, $\delta^{17}O$ values for each spot analyzed. (f) FeO-rich pyroxene fragment C2 from Sahara 97096 associated with silica and adjacent enstatite. Numbers in parentheses are $\Delta^{17}O$ values for each spot analyzed. (g) C23 from LEW 87223 consisting of FeO-rich pyroxene, enstatite and silica. Enstatite occurs both in the central region of the chondrule and on the edges. There is also a vein of enstatite that extends from the edge to the center. This chondrule also contains silica in association with the enstatite in the center.

chondrule also contains silica in association with the enstatite in the center (Fig. 2g).

There are some other textural features worthy of mention. None of the chondrules studied appears to have fine-grained rims as observed on chondrules in unequilibrated ordinary and carbonaceous chondrites. No fine-grained matrix was observed interstitial to the chondrules and if present, it is a very minor component. Additionally, no compound chondrules were observed.

3.2. Mineral compositions

Enstatite with near-endmember composition ($Fs_{<1}$) is dominant in most chondrules in E3 chondrites and this is true of many of the chondrules and fragments that we studied here (Table 1, Fig. 3). Minor element oxides MnO and Cr_2O_3 range from below detection (bd) to 0.6 and 0.8 wt.%, respectively. FeO-rich pyroxene has up to 12 wt.% FeO, with up to 0.9 MnO and 1.8 wt.% Cr_2O_3 (Table 1). FeO-rich pyroxene grains generally contain tiny (<1 μm) inclusions of Fe-metal and/or Fe-sulfide (Fig. 2g). Some show areas of low-Fe enstatite associated with the metal blebs suggesting reduction of Fe. In a previous study we used cathodoluminescence (CL) to identify three types of pyroxene in E3 chondrules (Weisberg et al., 1994). These include (1) pure (minor element-poor) enstatite (blue CL), (2) minor element-bearing enstatite (red CL) and (3) FeO-rich pyroxene (no CL). Some chondrules are disequilibrium assemblages of all three types. Fragment C2 from Sahara 97096 is an assemblage of FeO-rich pyroxene with minor silica and enstatite (Fig. 2f). C23 in LEW 87223 contains FeO-rich pyroxene and pure enstatite (Fig. 2g).

Olivine ranges from near pure forsterite ($Fa_{<1}$) up to Fa_{11} (Weisberg et al., 1994), with MnO from below detection (bd) to 0.5 wt.% and Cr_2O_3 from bd to 0.7 wt.% (Table 2). Mesostasis compositions are albitic with up to ~68 wt.% SiO_2, 18% Al_2O_3, 9% Na_2O and 5% CaO. Precise values are difficult to obtain due to the presence of microcrystals and Na migration (drop in counts) during electron probe analysis.

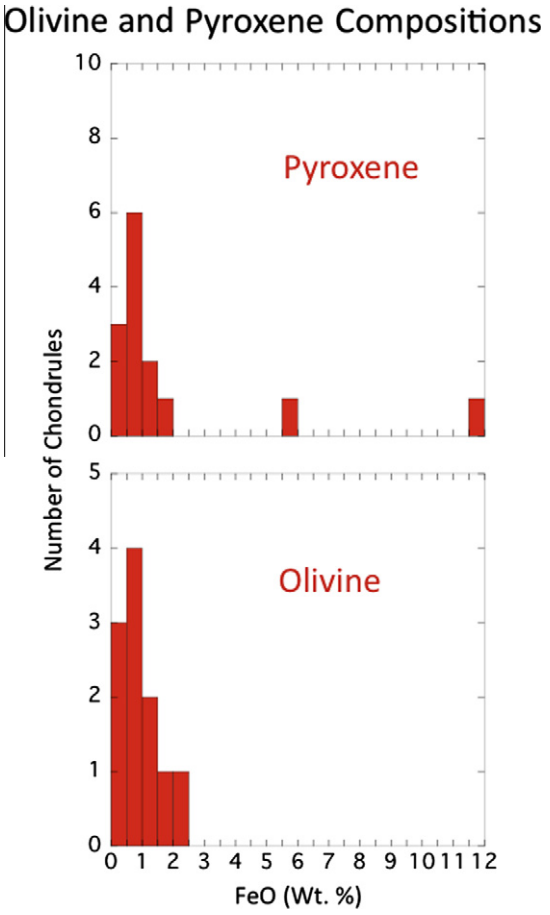

Fig. 3. Histogram showing the distribution of olivine and pyroxene compositions from the chondrules studied.

3.3. Oxygen isotopes

On the oxygen 3-isotope diagram individual bulk chondrules from EH3 chondrites have been shown to form a distinct cluster, not overlapping chondrules from ordinary or

Table 1
Representative compositions of pyroxene in E3 chondrules.

	Sahara 97096						Yamato 691				LEW 87223	
	C1	C2*	C3	C5	C6	C11	C1	C2	C5	C7	C23	C23
SiO_2	58.6	54.2	59.9	59.2	59.7	58.0	59.7	59.3	59.7	59.0	56.6	59.7
TiO_2	bd	bd	bd	bd	bd	0.21	0.13	0.07	bd	bd	bd	bd
Al_2O_3	0.31	0.23	bd	0.24	bd	0.73	0.44	0.21	0.43	0.92	0.24	0.15
Cr_2O_3	0.46	0.98	0.43	0.49	bd	0.35	0.23	0.11	bd	0.46	0.84	bd
FeO	1.4	10.5	0.68	0.83	0.26	1.2	0.64	0.33	0.37	0.64	10.7	0.55
MnO	0.17	0.18	0.08	0.15	bd	0.25	0.30	0.20	bd	0.05	0.39	bd
MgO	37.8	32.8	38.5	38.7	40.0	37.7	38.9	39.4	38.7	38.4	31.2	40.2
CaO	0.34	0.31	0.31	0.27	0.06	0.69	0.29	0.19	0.63	0.45	0.53	bd
Total	99.08	99.20	99.90	99.88	100.02	99.13	100.63	99.81	99.83	99.92	100.50	100.70
Fs	2.0	15.1	1.0	1.2	0.4	1.7	0.9	0.5	0.5	0.9	16.0	0.8
Wo	0.6	0.6	0.6	0.5	0.1	1.3	0.5	0.3	1.1	0.8	1.0	0.0

bd – below detection (<0.03). Na_2O was measured but was below detection (<0.08 wt.%).
* Mean of 12 points, FeO ranges 9.8–12.0 wt.%.

Table 2
Representative compositions of olivine in E3 chondrules.

	Sahara 97096					Yamato 691			
	C1	C3	C5	C6	C11	C1	C5	C7	C8
SiO_2	42.0	42.4	42.2	41.9	41.2–42.3	42.4	43.3	42.3	42.5
Cr_2O_3	0.13	0.36	0.35	0.33	0.26–0.44	0.24	0.14	0.32	0.32
FeO	0.95	0.69	1.6	1.3	1.4–3.5	0.46	0.39	1.2	2.1
MnO	0.15	0.12	0.11	0.09	0.05–0.25	0.33	0.12	0.04	0.14
MgO	55.9	56.2	55.6	55.4	54.2–56.4	56.0	56.0	55.3	54.9
CaO	0.22	bd	bd	0.29	0.15–0.28	0.17	0.13	0.22	0.08
Total	99.35	99.77	99.86	99.31		99.60	100.08	99.38	100.04
Fa	0.9	0.7	1.6	1.3	1.4–3.4	0.5	0.4	1.2	2.1

TiO_2 and Al_2O_3 were analyzed but were all below detection limits (<0.03 wt.%).
Na_2O was analyzed but was below detection (<0.08 wt.%).

carbonaceous chondrites (Clayton et al., 1977; Clayton and Mayeda, 1984; Weisberg et al., 1994). Our *in situ* SIMS data show that most E3 pyroxene (mineral fragments and in chondrules) plots near the terrestrial fractionation (TF) line similar to whole rock data (Table 3, Figs. 4a–d, 5 and 6). However, some enstatite in LEW 87223 and Sahara 97096 plots above the TF line, near the OC field (Fig. 4a and c) with the $\Delta^{17}O$ values as high as 1‰.

Most FeO-rich pyroxene plots on the TF line within analytical uncertainties, similar to most of the enstatite (Fig. 4c and 5). In LEW 87223 C21, both the FeO-rich pyroxene and the enstatite have identical oxygen isotope ratios. In C23, the FeO-rich pyroxene has oxygen isotope ratios that plot on the terrestrial fractionation line similar to whole rock compositions but the enstatite is different having higher $\Delta^{17}O$ values, similar to ordinary chondrites (Table 3, Figs. 4c and 5).

Olivine shows a wide range of oxygen isotope ratios with $\Delta^{17}O$ values from below −4‰ to 2.3‰ (Table 3, Fig. 5). The majority of olivine data plots on the TF line similar to the enstatite and whole rock compositions (Figs. 4 and 5). Noteworthy is the large central olivine in C11 from Sahara 97096 (Fig. 2c and d) that plots at high $\Delta^{17}O$ values close to the R chondrites (Fig. 4a). The surrounding pyroxene, however, plots on the TF line similar to other pyroxene grains from E chondrites (Fig 4a). Olivine data from LEW 87223 C1 and Y 691 C1 show a large variation in $\delta^{18}O$ and $\delta^{17}O$ ratios below the TF line and appear to define a unique mixing line similar to but displaced from the CCAM line (Figs. 4b and 6). A linear regression through all of the data from these two chondrules yields a well-correlated line with a formula $\delta^{17}O = (0.95 \pm 0.06) \times \delta^{18}O - (2.3 \pm 0.3)$, which is almost parallel to CCAM line. The average of most E3 data, excluding those with ordinary and R chondritic oxygen isotope ratios, is calculated to be $\delta^{18}O$ and $\delta^{17}O$ of 4.9 ± 1.4‰ and 2.3 ± 1.3‰, respectively, and it plots on the regression line determined from the two chondrules (Figs. 4b and 6a). We refer to this line as the enstatite chondrite mixing (ECM) line (Fig. 6a). Ushikubo et al. (2011) found that the minerals in chondrules from Acfer 094 plot along a single line, which lies between the CCAM and the TF lines that has a slope of 0.987 ± 0.013 with an intercept of -2.7 ± 0.1‰. Ushikubo et al. (2011) referred to this line, defined by minerals in Acfer 094 chondrules, as the primitive chondrule mineral (PCM) line. The ECM line obtained from this work may be similar or related to the PCM line.

Olivine from Al-rich chondrule LEW 87223 C2 plots near but slightly above the terrestrial fractionation line and at higher $\delta^{18}O$ values (Fig. 4a). Oxygen isotope ratios for olivine bars from BO chondrule Sahara 97096 C1 also plots on the TF line but shows a range of $\delta^{18}O$ values from 3.69 to 5.10 indicating internal mass fractionation (Fig. 4d). There does not appear to be any textural or compositional difference between these olivine bars.

4. DISCUSSION

4.1. Origin of olivine in E3 chondrite chondrules

Olivine is present in enstatite chondrites of low petrologic grade and is rare to absent in petrologic types greater than E4. It makes up to 7.4 vol.% of EH3 chondrites (Weisberg et al., 1994). In some E3 chondrules, the textural setting of olivine suggests that it may be a relict grain. However, in most of the chondrules that we studied the olivine Mg# and oxygen isotope ratios are indistinguishable from those of the enstatite. Many of the olivine grains have $\Delta^{17}O \sim 0$ (e.g., Table 3, Fig 5) similar to whole rock E chondrite compositions (e.g., Weisberg et al., 1994). This suggests formation of the olivine in the E chondrite chondrule-forming region. Olivine in chondrules from O or C chondrites have $\Delta^{17}O \sim 0$ in only a few rare cases (e.g., Jones et al., 2004; Chaussidon et al., 2008; Kita et al., 2010; Ushikubo et al., 2011).

Some olivine, however, shows a variable $\Delta^{17}O$ value, which is different from that in the pyroxene in the same chondrule. In chondrule Y 691 C7, the oxygen isotope ratio of enstatite plots on the TF line near whole rock compositions and the olivine has a range of compositions plotting below the TF line, between the TF line and the CCAM lines (Fig. 4a). Compositionally the olivine is very magnesian with an Mg# similar to the enstatite in the same chondrule. Texturally the olivine occurs in the center of the chondrule as phenocrysts and the enstatite occurs on the edges of the chondrule, poikilitically enclosing some of the olivine (Fig. 2b). The mixtures of these minerals with differing oxy-

Table 3
Oxygen isotope compositions of olivine (Ol), enstatite (En) and Fe-bearing pyroxene (Fe-pyx) in E3 chondrules.

Sample	Texture	Spot	Phase	Avg. Mg#	$\delta^{18}O$	Error	$\delta^{17}O$	Error	$\Delta^{17}O$	Error	Average chondrule
Sah 97096 C1	BO	C1-1	Ol	0.992	3.60	0.15	1.91	0.30	0.03	0.33	Y
		C1-2	Ol		4.45	0.15	2.12	0.30	−0.19	0.33	Y
		C1-3	Ol		5.10	0.15	2.55	0.30	−0.10	0.33	Y
		C1-4	Ol		3.77	0.15	2.08	0.30	0.12	0.33	Y
		Average ($n = 4$)			4.23	0.69	2.17	0.27	−0.03	0.16	
Sah 97096 C2	F	C2-1	Fe-pyx	0.832	3.09	0.15	0.98	0.30	−0.63	0.33	
		C2-4	Fe-pyx		2.92	0.30	0.86	0.46	−0.66	0.49	
		C2-6	Fe-pyx		3.74	0.30	0.99	0.46	−0.96	0.49	
		C2-2	Fe-pyx		3.56	0.15	2.13	0.30	0.28	0.33	
		C2-5	Fe-pyx		3.61	0.30	1.84	0.46	−0.04	0.49	
		C2-3	En	0.982	4.29	0.15	2.06	0.30	−0.17	0.33	Y
		Average spots −1, −4, −6 ($n = 3$)			3.25	0.50	0.94	0.27	−0.75	0.28	
		Average spots −2, −5 ($n = 2$)			3.58	0.30	1.98	0.33	0.12	0.35	
Sah 97096 C3	POP	C3-1	Ol	0.988	4.99	0.15	2.54	0.30	−0.06	0.33	Y
		C3-3	Ol	0.989	5.23	0.15	3.08	0.30	0.36	0.33	Y
		C3-2	En	0.987	4.53	0.15	2.98	0.30	0.62	0.33	Y
Sah 97096 C5	POP	C5-1	Ol	0.984	5.32	0.15	2.79	0.30	0.02	0.33	Y
		C5-3	Ol		5.82	0.15	2.56	0.30	−0.47	0.33	Y
		C5-2	En	0.982	4.75	0.15	1.99	0.30	−0.48	0.33	Y
Sah 97096 C6	POP	C6-1	Ol	0.984	5.10	0.30	2.50	0.46	−0.15	0.49	Y
		C6-2	En	0.994	4.69	0.30	2.86	0.46	0.42	0.49	Y
Sah 97096 C10	POP	C10-1	Ol	0.987	6.10	0.30	2.45	0.46	−0.72	0.49	Y
		C10-2	Ol		5.76	0.30	2.65	0.46	−0.34	0.49	Y
		C10-3	En	0.985	5.54	0.30	2.44	0.46	−0.44	0.49	Y
		Average Ol ($n = 2$)			5.93	0.35	2.55	0.33	−0.53	0.38	
Sah 97096 C11	POP	C11-1	Ol	.976–.986	4.84	0.30	4.68	0.46	2.16	0.49	
		C11-2	Ol		4.82	0.30	4.81	0.46	2.31	0.49	
		C11-3	En	0.975	4.81	0.30	2.73	0.46	0.23	0.49	Y
		Average Ol ($n = 2$)			4.83	0.30	4.74	0.33	2.23	0.35	
Sah 97096 C12	POP	C12-1	Ol	0.989	5.37	0.30	2.26	0.46	−0.53	0.49	Y
		C12-2	En	0.989	5.41	0.30	2.49	0.46	−0.32	0.49	Y
Sah 97096 C15	MF	C15-1	En		5.60	0.30	2.58	0.46	−0.33	0.49	Y
LEW 87223 C23	PP	C23-1	Fe-pyx	0.893	3.25	0.31	1.90	0.64	0.21	0.67	
		C23-2	Fe-pyx		3.58	0.31	2.12	0.64	0.26	0.67	
		C23-6	Fe-pyx		3.68	0.31	1.72	0.64	−0.19	0.67	
		C23-3	En	0.984	4.78	0.31	3.42	0.64	0.94	0.67	
		C23-4	En		4.64	0.31	3.19	0.64	0.77	0.67	
		C23-5	En		4.63	0.31	3.77	0.64	1.37	0.67	
		Average Fe-pyx (n = 3)			3.50	0.30	1.91	0.37	0.09	0.39	
		Average En ($n = 3$)			4.68	0.30	3.46	0.37	1.03	0.39	
LEW 87223	MF	LEW 87223 MF-1	En	0.993	5.19	0.31	3.92	0.64	1.21	0.67	Y
		LEW 87223 MF-2	En	0.994	4.67	0.31	2.09	0.64	−0.34	0.67	Y
LEW 87223 C21	PP	C21-1	Fe-pyx		3.86	0.31	1.99	0.64	−0.01	0.67	
		C21-2	En		3.96	0.31	2.20	0.64	0.14	0.67	Y
LEW 87223 C1	POP	C1-1	Ol	0.999	4.72	0.31	2.40	0.64	−0.05	0.67	
		C1-3	Ol		5.29	0.31	2.12	0.64	−0.63	0.67	
		C1-5	Ol		4.16	0.31	1.66	0.64	−0.50	0.67	
		C1-6	Ol		5.17	0.31	2.14	0.64	−0.55	0.67	
		C1-2	Ol		2.02	0.31	−0.49	0.64	−1.54	0.67	
		C1-4	En	0.994	4.17	0.31	1.69	0.64	−0.48	0.67	
		Average Ol ($n = 4$, excl. C1-2)			4.83	0.51	2.08	0.32	−0.43	0.33	

(*continued on next page*)

Table 3 (*continued*)

Sample	Texture	Spot	Phase	Avg. Mg#	$\delta^{18}O$	Error	$\delta^{17}O$	Error	$\Delta^{17}O$	Error	Average chondrule
LEW 87223 C14	PO, glass-rich	LEW 87223 C14-1	Ol	0.999	6.20	0.31	3.51	0.64	0.29	0.67	Y
Y 691 C1	POP	C1-1	Ol	0.996	−2.57	0.43	−4.44	0.54	−3.10	0.37	
		C1-3	Ol		−4.58	0.43	−6.68	0.54	−4.30	0.37	
		C1-4	Ol		3.99	0.43	1.04	0.54	−1.04	0.37	
		C1-7	Ol		4.11	0.43	1.77	0.54	−0.36	0.37	
		C1-5	Dusty Ol	0.996	5.41	0.43	2.69	0.54	−0.12	0.37	
		C1-2	En	0.994	5.54	0.43	3.42	0.54	0.55	0.37	
		C1-6	En		5.46	0.43	3.26	0.54	0.42	0.37	
		Average En ($n = 2$)			5.50	0.31	3.34	0.38	0.48	0.26	
Y 691 C2	MF	C2-1	En	0.987	5.24	0.43	2.57	0.54	−0.16	0.37	Y
Y 691 C3	MF	C3-1	En	0.916	3.88	0.43	2.09	0.54	0.07	0.37	Y
		C3-2	En		4.42	0.43	1.79	0.54	−0.51	0.37	Y
Y 691 C5	POP	C5-1	Ol	0.999	5.23	0.43	2.61	0.54	−0.11	0.37	Y
		C5-2	Ol		5.49	0.43	3.07	0.54	0.21	0.37	Y
		C5-3	En	0.999	4.51	0.43	1.99	0.54	−0.35	0.37	Y
		Average Ol ($n = 2$)			5.36	0.31	2.84	0.46	0.05	0.32	
Y 691 C6	PP	Y 691 C6-1	En	0.999	4.08	0.33	1.87	0.45	−0.26	0.56	Y
		Y 691 C6-2	En		4.66	0.33	2.10	0.45	−0.32	0.56	Y
		Average En ($n = 2$)			4.37	0.58	1.98	0.32	−0.29	0.40	
Y 691 C7	POP	Y 691 C7-1	Ol	0.988	5.07	0.33	1.55	0.45	−1.09	0.56	Y
		Y 691 C7-2	Ol		4.63	0.33	0.75	0.45	−1.66	0.56	Y
		Y 691 C7-3	Ol		3.91	0.33	0.75	0.45	−1.29	0.56	Y
		Y 691 C7-6	Ol		3.97	0.33	1.42	0.45	−0.64	0.56	Y
		Y 691 C7-4	En	0.991	3.89	0.33	1.88	0.45	−0.14	0.56	Y
		Y 691 C7-5	En		3.85	0.33	1.80	0.45	−0.21	0.56	Y
		Average En ($n = 2$)			3.87	0.30	1.84	0.32	−0.17	0.40	
Y 691 MF	MF	MF-1	Fe-pyx		5.48	0.33	3.14	0.45	0.29	0.56	Y
Y 691 C8	POP	C8-1	Ol	0.977	5.44	0.33	2.30	0.45	−0.53	0.56	Y
		C8-2	Ol		5.80	0.33	2.89	0.45	−0.13	0.56	Y
		Average Ol ($n = 2$)			5.62	0.36	2.59	0.59	−0.33	0.40	
Average of typical EC chondrules (marked as Y)					4.87	1.39	2.34	1.26	−0.20	0.99	

Sah – Sahara, LEW – Lewis Cliff, Y – Yamato.
F – fragment, MF – mineral fragment.
BO – barred olivine, POP – porphyritic olivine and pyroxene, PP – porphyritic pyroxene, PO – porphyritic olivine.
Mg# – Mg/(Mg + Fe) (in at.%).
The errors assigned to each spot analysis are 2SD of bracketing San Carlos olivine standard.
The average values of multiple spots are calculated in individual mineral phases for data set with indistinguishable $\Delta^{17}O$ values.
The error assigned for the average values are either 2SD of the mean or weighted errors.
The error of average $\delta^{18}O$ values should not be smaller than 0.3‰, which represent the uncertainties of matrix corrections (Kita et al., 2009).

gen isotope ratios within the same chondrule, implies incomplete melting of that chondrule and preservation of an oxygen isotope signature from an earlier oxygen reservoir. The outer enstatite-rich portion of C7 may have been remelted and/or equilibrated with the ambient E chondrite oxygen reservoir ($\Delta^{17}O = 0$) whereas the internal olivine did not.

In chondrule LEW 87223 C1 and Y 691 C1, the olivine grains are magnesian in composition but plot toward more ^{16}O-rich compositions than most enstatite and other E3 olivine (Figs. 4b and 6a). The O-isotope ratios of olivine in these chondrules helps form a line that extends from the main cluster of oxygen isotope ratios for E3 olivine and pyroxene down to the $\Delta^{17}O = -4‰$ (olivine in Y 691 C1). This line (ECM) is approximately parallel to but displaced from the CCAM line. The ECM line appears to coincide with a line defined by chondrules from Acfer 094 referred to as the PCM (primitive chondrite mineral) line by Ushikubo et al. (2011). A ^{16}O-rich chondrule mixing trend very similar to that from this study was also found in LL3 and H3 chondrites (Kita et al., 2008, 2010). This suggests that this mixing line may be common for many primitive materials and that the O, C, and E chondrite forming regions may have shared common precursor solids.

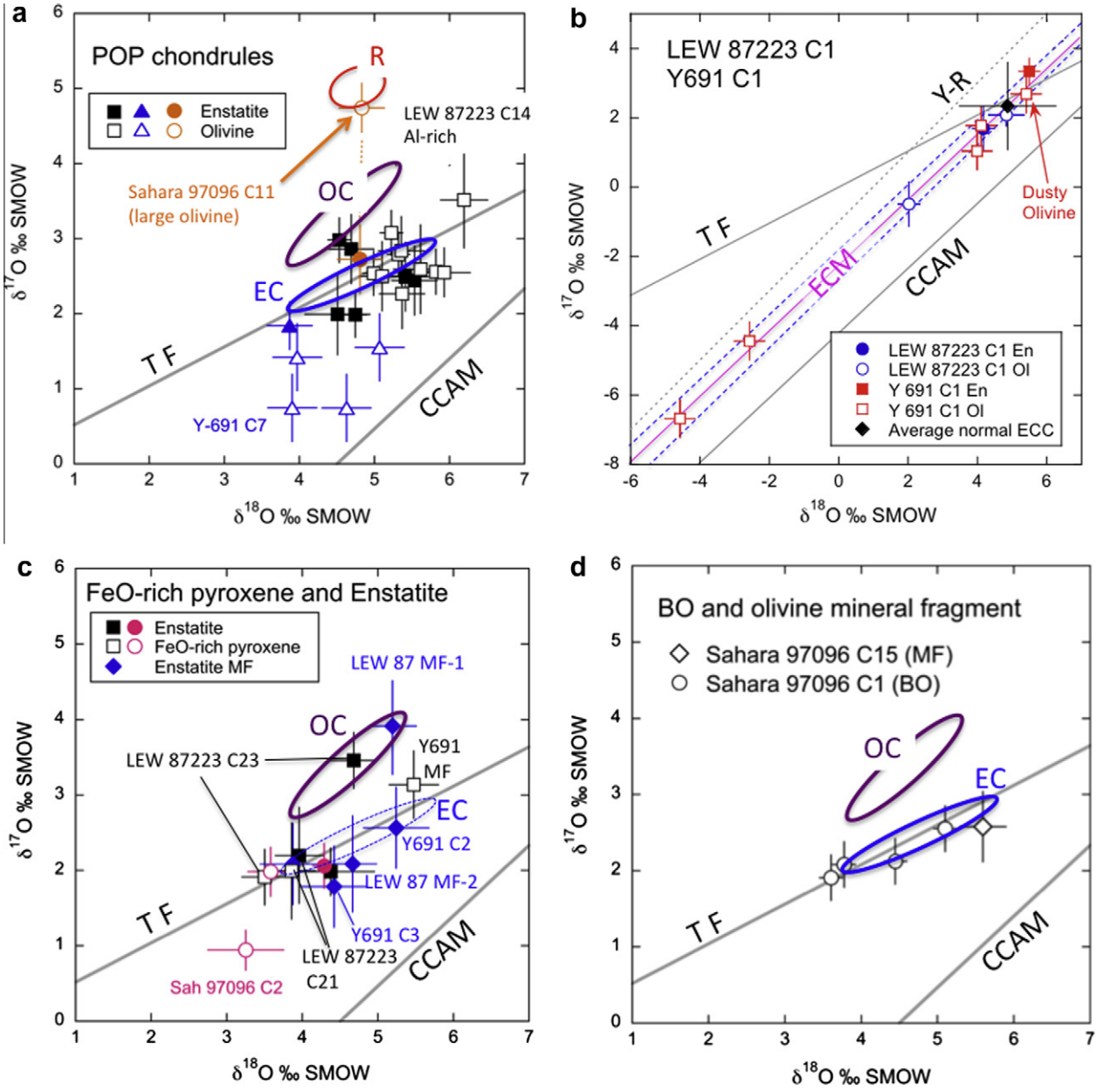

Fig. 4. Oxygen 3-isotope diagrams showing oxygen isotope ratios of the olivine and pyroxene analyzed from chondrules and fragments in Sahara 97096, Y 691 and LEW 87223. (a) Porphyritic olivine pyroxene (POP) chondrules in E3 chondrites. Olivine and enstatite plot along the terrestrial fractionation (TF) line overlapping the range for E chondrite whole rocks (EC). Some enstatite plots above near the light oxygen end of the compositions of ordinary chondrites (OC). Olivine from Y691 C7 plots below the TF line. The large olivine from C11 (Fig. 1c and d) plots near the compositions of R chondrites whereas the enstatite from C11 plots near the main cluster for the chondrules, near the TF line. (b) Porphyritic olivine pyroxene (POP) chondrules C1 from Y 691 ad C1 from LEW 87223. The two chondrules have oxygen isotope ratios that cross the E chondrite whole rock region on the TF line but extend down toward more ^{16}O-rich compositions. The data from these chondrules yield a well-correlated line with a formula $\delta^{17}O = (0.95 \pm 0.06) \times \delta^{18}O - (2.3 \pm 0.3)$, which is almost parallel to the CCAM line. The average of most enstatite chondrite chondrule data (average normal ECC), excluding those with ordinary and R chondritic oxygen isotope ratios, is calculated to be $\delta^{18}O$ and $\delta^{17}O$ of $4.9 \pm 1.4‰$ and $2.3 \pm 1.3‰$, respectively, and plots on the regression line determined from the two chondrules. We refer to this line as the enstatite chondrite mixing (ECM) line. Also plotted is the error envelope (dashed blue lines) for the ECM. (c) Chondrules and mineral fragments containing FeO-rich pyroxene. Most FeO-rich pyroxene plots on the TF line similar to the majority of enstatite. However, enstatite associated with FeO-rich pyroxene in LEW 87223 C23 and MF-1 plot above the TF in the ordinary chondrite (OC) region of the diagram. (d) Barred olivine (BO) chondrule and a olivine mineral fragment from Sahara 97096. These olivine plot on the terrestrial fractionation but show a range of $\delta^{18}O$ values. (For interpretation of the references to color in this figure legend, the reader is referred to the web version of this article.)

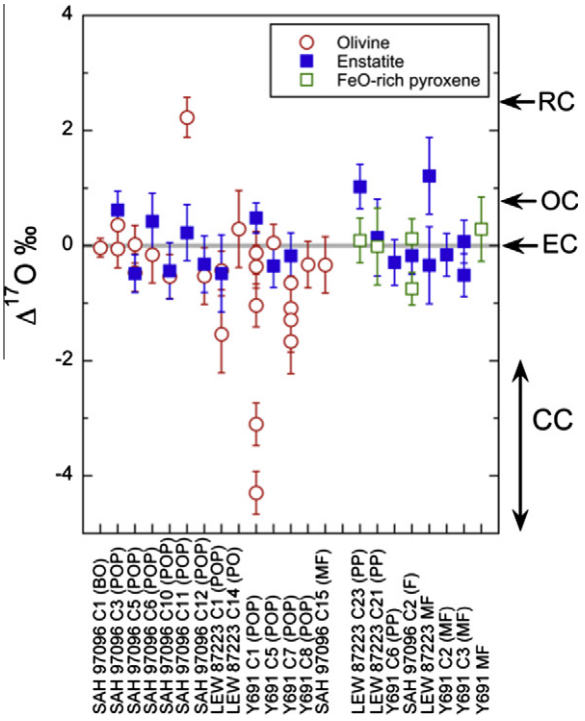

Fig. 5. Plot of $\Delta^{17}O$ values for the olivine, enstatite and FeO-rich pyroxene in the E3 chondrites showing that most of these minerals have $\Delta^{17}O$ values close to 0. Olivine shows a range of values from below −4 to 2.3‰.

The large olivine grain in C11 from Sahara 97096 (Fig. 2c and d) is out of textural and compositional equilibrium with the surrounding finer-grained enstatite and silica in this chondrule. Its oxygen isotope ratios are not only unusual for this particular chondrule but for any of the materials in an E chondrite (Fig. 4a). The $\Delta^{17}O$ value of the olivine (2.2 ± 0.4‰) is higher than those in LL3 chondrite chondrules (Kita et al., 2010) and close to the range of R chondrites. Thus, we interpret this to be a relict grain that formed in an earlier chondrule-forming event and that survived melting of C11. The origin of this grain and its relationship to other materials in the E chondrites is not clear. It could be a foreign grain that was mixed into the E chondrite region.

4.2. The relationship of FeO-rich pyroxene to enstatite in E3 chondrites

FeO-rich pyroxene (defined as having >2 wt.% FeO) is minor in the unequilibrated enstatite chondrites and rare to absent in more equilibrated E4-6 chondrites (Leitch and Smith, 1982; Lusby et al., 1987; Weisberg et al., 1994; Kimura et al., 2003). Many of the FeO-rich pyroxene grains have oxygen isotope ratios that plot near the TF line on the oxygen 3-isotope diagram similar to whole rock compositions and to the more reduced minerals (e.g., enstatite) that are typical of E chondrites. Similar results were reported by Kimura et al. (2003) though the precisions of their analyses were fairly limited (at the level ⩾2‰ in 2SD). Our new data

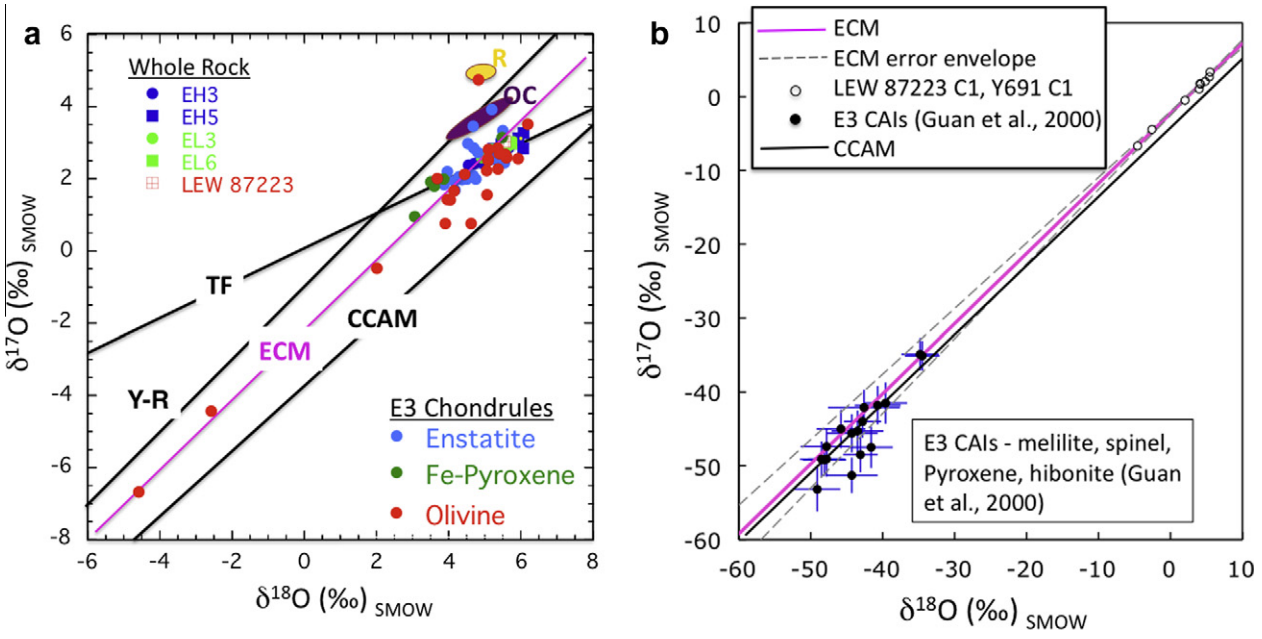

Fig. 6. (a) Oxygen isotope summary diagram showing ratios for all of the olivine and pyroxene grains that we analyzed in the three E3 chondrites. Most grains plot along the terrestrial fractionation (TF) line similar to E chondrite whole rock compositions. Some grains plot near the ordinary chondrites, the large relict olivine from C11 plots near the R chondrites. Olivine from some chondrules appear to form a mixing line similar to but displaced from the CCAM (carbonaceous chondrite anhydrous mixing) line. Also plotted is the ECM (enstatite chondrite mixing) line from Fig. 4b. (b) Oxygen isotope summary diagram showing our data for chondrules from E3 chondrites in comparison to the ^{16}O-rich compositions of refractory inclusions from E3 chondrites (Guan et al., 2000). Also shown is an extension of the ECM drawn toward the ^{16}O-rich compositions of the refractory inclusions. Dashed lines represent the error envelope for the ECM.

at sub-‰ precision show a tighter distribution of both FeO-rich pyroxene and enstatite that overlaps each other.

In some cases FeO-rich pyroxene and enstatite from the same chondrule have different oxygen isotope ratios, such as C23 in LEW 87223 (Table 3, Fig. 4c). In other cases the FeO-rich pyroxene and the enstatite in the same chondrule have the same oxygen isotope ratios, such as C21 in LEW 87223 (Table 3, Fig. 4c). The enstatite in C23, which is near-pure in composition, occurs on the outer edge of the chondrule, as veins in the FeO-rich pyroxene, and in the chondrule interior. Although the enstatite occurs in the interior of the chondrule, there is a vein leading from the enstatite in the interior to the outer portion of the chondrule. This chondrule was studied by Weisberg et al. (1994) and they interpreted the enstatite to have formed later than the FeO-rich pyroxene. The oxygen isotope composition of the enstatite in C23 is unusual in that it plots above the TF line with $\Delta^{17}O = 1.0‰$ (Figs. 2g and 4c). An enstatite mineral fragment from LEW 87223 also has a relatively high $\Delta^{17}O$ value of 1.2‰ (Figs. 4c and 5).

In the case of C21 the enstatite and FeO-rich pyroxene have the same oxygen isotope ratios. The enstatite in C21 may have formed through reduction of Fe from pyroxene similar to the remaining FeO-rich pyroxene in this chondrule (e.g., Weisberg et al., 1994). Thus, in some cases, the FeO-rich pyroxene and the enstatite in the E3 chondrites may have formed at different times under different redox conditions but from the same oxygen reservoir, as also concluded by Kimura et al. (2003).

4.3. Oxygen isotope heterogeneity and evidence of relict grains in E3 chondrules

Relict grains that survived chondrule melting have been identified in chondrules from E, O and C chondrites. They are generally identified as grains having petrologic features that are in gross petrologic and chemical disequilibrium with their host chondrule. For example, FeO-rich grains in type I chondrules were among the first materials interpreted to be relict crystals (e.g., Nagahara, 1981, 1983). Mg-rich relicts in type II, FeO-rich chondrules have also been identified and in some cases, have been shown to have more ^{16}O-rich oxygen isotope compositions than other minerals in the same chondrule (Rambaldi, 1981; Yurimoto and Wasson, 2002; Kunihiro et al., 2004, 2005; Ushikubo et al., 2011).

Grains of FeO-rich pyroxene and olivine, some of which have dusty inclusions, have been indentified in E chondrite chondrules (Leitch and Smith, 1982; Lusby et al., 1987; Weisberg et al., 1994; Kimura et al., 2003). In the chondrules and fragments that we studied, some of the FeO-rich grains contain dusty inclusions (e.g., LEW 87223 C21 and C23, Fig. 2g). However, the oxygen isotope ratios of the FeO-rich pyroxene are not different from the enstatite in C21 and both have isotope ratios that plot on the TF line (Fig. 4c). In C23 from LEW 87223 (Fig. 2g) the FeO-rich pyroxene and the enstatite have different oxygen isotope ratios as discussed above and shown in Fig. 4c.

In Y 691 C1, one olivine has dusty metal inclusions and the olivine in this chondrule shows a range of oxygen isotope ratios (Fig. 4b). The dusty olivine has an oxygen isotope ratio that plots within error of the TF line suggesting that it formed in the enstatite chondrite source region (Fig. 4b). Other olivine grains in C1 have more ^{16}O-rich compositions forming the ECM line, as discussed above. The range of oxygen isotope ratios suggests incomplete melting of this chondrule.

The large olivine grain in C11 from Sahara 97096 (Fig. 2c and d) is out of textural and compositional equilibrium with the surrounding finer-grained enstatite and silica in this chondrule. Its oxygen isotope ratios are unusual in being similar to those of R chondrites (Fig. 4a). Thus, we interpret this to be a relict grain that formed in an earlier chondrule-forming event. It suggests incomplete melting for chondrule C11, survival of minerals from previous generations of chondrules, and chondrule recycling as proposed for chondrules in other chondrite groups (e.g., Jones, 1996).

4.4. Oxygen isotopes of E3 chondrules

The silicates in E3 chondrules show a range of O isotope ratios. Although most enstatite, the dominant mineral in most E3 chondrules, has isotope ratios that plot on the TF line near whole rock compositions, some plot above the TF line in the OC region of the 3-isotope diagram. Most FeO-rich pyroxene plots on the TF line with most of the Fe-poor enstatite, suggesting both formed locally in the EC region and was most likely not transported from the O chondrite or other chondrule-forming regions. Thus, oxidation/reduction conditions varied widely within the E chondrite nebular region. Kimura et al. (2003) drew a similar conclusion based on their limited oxygen isotope analyses of FeO-rich pyroxene in E3 chondrites. Olivine shows a range of compositions from high $\Delta^{17}O$ to ^{16}O-rich values and forms a mixing (ECM) line parallel to but distinct from the CCAM line. The majority of oxygen isotope ratios of minerals in the E3 chondrules form a cluster on the terrestrial fractionation line similar to whole rock E chondrite compositions (Weisberg et al., 1994). The ECM line, discussed above, intersects this cluster of oxygen isotope ratios (Fig. 5a) and the cluster of data on the TF line may represent the composition of the ambient E chondrite nebular gas.

The oxygen isotope ratios of barred olivine chondrules are thought to represent the composition of the ambient nebular gas because BO chondrules formed by complete melting of their precursors (e.g., Clayton et al., 1977; Chaussidon et al., 2008). The BO chondrule we studied (C1 from Sahara 97096) has oxygen isotope ratios that plot within error of the TF line (average $\Delta^{17}O = -0.03 \pm 0.16‰$, $n = 4$, Figs. 4d and 5). Additionally, this chondrule exhibits internal mass dependent fractionation in $\delta^{18}O$ with constant $\Delta^{17}O$ (Table 3, Fig. 4d). Kita et al. (2010) suggested open system (gas–solid oxygen isotope exchange) behavior to explain large mass-dependent fractionations that they observed in Type IA chondrules in LL3 chondrites. In their model evaporation and recondensation of chondrule precursor solids caused large mass-dependent fractionation in the Type IA chondrules due to kinetic fractionation during

condensation or equilibrium fractionation between gas and solid. In C1 the heaviest oxygen seems to be in the interior. The interior of the chondrule may have preserved the average dust oxygen isotope ratios and olivine closer to the rim interacted with the surrounding gas. However, more data from this chondrule would be needed to test this hypothesis.

The isotopic ratios of the olivine in the Al-rich chondrule (LEW 87223 C14) plots near the TF line similar to most minerals in the E3 type I chondrules (Fig. 4a) and thus, formed in the same region as the other E chondrite chondrules. Although some Al-rich chondrules in O chondrites show very ^{16}O-rich signatures (Russell et al., 2000), one Al-rich chondrule in an LL3 (Kita et al., 2010) and an Al-rich chondrule in Acfer 094 (Ushikubo et al., 2011) show the same oxygen isotope ratios as type I chondrules in the same meteorites.

The range of O isotope compositions and mixing behavior in E3 chondrules is similar to that in other chondrite groups, indicating similar chondrule-forming processes, gas–melt exchange, and that some chondrule precursors included ^{16}O-rich solids. However, the clustering of data about the TF line (Fig. 6) suggests the oxygen isotope reservoir in the local nebular region was different from that of other chondrite groups. The petrologic characteristics of the chondrules, such as the reduced compositions of most silicates, and in some chondrules presence of silica, Si-bearing metal and oldhamite (e.g., Weisberg et al., 1995) indicates that the chondrules formed under more reducing conditions than type I chondrules from other groups. The lack of fine-grained matrix and fine-grained chondrule rims in E chondrites may indicate that the chondrule forming process (melting of dust) may have been more efficient than in the O or C chondrite regions. Thus, the E chondrites are products of a distinct nebular environment.

4.5. Relationship of the chondrules to calcium-aluminum-rich inclusions (CAIs) in E3 chondrites

The oxygen isotope ratios of CAIs in E3 chondrites have been measured previously and their constituent minerals (hibonite, pyroxene and spinel) have very ^{16}O-rich compositions and appear to plot on the CCAM line, similar to CAIs in carbonaceous chondrites (Guan et al., 2000; Fagan et al., 2001 and Lin et al., 2003; Fig. 6b). Olivine and pyroxene in the E chondrite chondrules appear to form their own (ECM) line which is approximately parallel to but distinct from the CCAM line. Unfortunately it is not possible to statistically distinguish the ECM line from the CAI data. However, the CAIs in E3 chondrites are petrologically and oxygen isotopically similar to the CAIs described in other chondrites and do not appear to be unique to the E chondrites (Guan et al., 2000; Fagan et al., 2001; Lin et al., 2003). Therefore, they may have formed in the same nebular region or the same event as the CAIs in other chondrite groups, as suggested previously (e.g., Guan et al., 2000; Fagan et al., 2001; Lin et al., 2003) and were later incorporated into the E chondrite region.

If the chondrules and CAIs formed from different oxygen reservoirs and the chondrules represent an oxygen reservoir that differs from chondrules in other groups, it suggests that chondrule formation was a local event, but CAI formation was not. Each chondrite group seems to contain the chondrules that formed in their own local region suggesting that chondrules are local products. This is further supported by the petrologic differences between the chondrules in E3 chondrites and those in the other chondrite groups, such as highly reduced mineral compositions, the presence of Si-bearing metal, Cr-bearing troilite and oldhamite. CAIs, however, may have all formed in the same region and were later distributed by a mechanism such as radial transport (e.g., Ciesla, 2007) or disk winds (e.g., Shu et al., 1995) to the various chondrule-forming regions. This also implies that there was transport of materials following CAI formation but transport mechanisms were less active following chondrule formation; E chondrite-like chondrules are not found in O or C chondrites.

The large gap in oxygen isotope composition between CAIs and chondrules in E3 chondrites also argues against a relationship between them (Fig. 6b). However, if the ECM is interpreted to be the result of mixing between ^{16}O-rich CAI-like solids and the ^{16}O-depleted ambient gas, the array of compositions along the ECM (e.g., Fig. 4b) can be understood by models of photo-dissociation (e.g., Yurimoto and Kuramoto, 2004). In the model of Yurimoto and Kuramoto (2004) icy bodies became enriched in ^{17}O and ^{18}O through isotopic self-shielding during ultraviolet photo-dissociation of CO in the protosolar molecular cloud. Introduction of the ice into the inner solar system may have resulted in the ^{16}O-poor E chondrite gas reservoir. The ECM may be the result of mixing between the ^{16}O-rich solids and the ^{16}O-poor reservoir.

Further work on more olivine and pyroxene in EH3 chondrules may provide data to further define the ECM line and help understand the relationship between chondrules and CAIs. Additionally data on EL3 chondrules may help to better understand the distribution of oxygen isotope compositions in E chondrites.

5. CONCLUSIONS

(1) Chondrules in E3 chondrites can be considered to be type I chondrules but differ from those in other chondrite groups. Many contain near-pure endmember enstatite ($Fs_{<1}$). Some contain a silica phase, Si-bearing FeNi metal, Cr-bearing troilite and in some cases Mg, Mn- and Ca-sulfides. Olivine and more FeO-rich pyroxene grains are present in some chondrules but are much less common than in ordinary or carbonaceous chondrite chondrules.

(2) The oxygen isotope ratios of olivine and pyroxene in E3 chondrules show a wide range of values as large as 10‰ in both δ^{18}O and δ^{17}O. Most enstatite data plot on the TF line near whole rock data, while some plots above in the OC region of the oxygen three-isotope diagram.

(3) Most FeO-rich pyroxene data plot on the TF line similar to enstatite, suggesting it formed locally in the EC region and was not transported from the

OC or other chondrule-forming region. Thus, oxidation/reduction conditions varied within the E3 chondrule-forming region.

(4) Olivine shows a wide range of $\Delta^{17}O$ values ($-4‰$ to $+2‰$). A linear regression through the data from two olivine-bearing chondrules yields a well-correlated line with a formula $\delta^{17}O = (0.95 \pm 0.06) \times \delta^{18}O - (2.3 \pm 0.3)$, which is almost parallel to the CCAM line. We refer to this as the ECM line but it also may coincide with a line defined by chondrules from Acfer 094 referred to as the PCM (Primitive Chondrite Mineral) line (Ushikubo et al., 2011).

(5) Chondrules in E3 chondrites contain ^{16}O-rich precursors that might be common to solid precursors of the chondrules in carbonaceous chondrites and minor chondrules in ordinary chondrites.

(6) Oxygen isotope heterogeneity was found in minerals from some of the chondrules in E3 chondrites. This suggests incomplete melting of the chondrules, survival of minerals from previous generations of chondrules, and chondrule recycling. The presence of R chondrite-like oxygen in a large, possibly relict, olivine is perplexing and requires further exploration. It may indicate limited mixing of materials from other reservoirs.

(7) The CAIs in E3 chondrites have petrologic characteristics and oxygen isotope compositions similar to those in other chondrite groups, and appear to have formed in a different oxygen reservoir from the chondrules. Therefore we conclude that chondrule formation was a local event but CAIs may have all formed in one distinct place and time and were later redistributed to the various chondrule-forming and parent body accretion regions. This also implies that there was transport of materials following CAI formation but transport mechanisms were less active at the time of and following chondrule formation.

ACKNOWLEDGEMENTS

We thank Charlie Mandeville, Joe Boesenberg and Robert Schenck for technical support. We are grateful to M. Petaev, K. Nagashima and H. Yurimoto for helpful reviews and to A. Krot for editorial handling. This project was supported by NASA Cosmochemistry Grants NNX09AG94G (M.K. Weisberg, P.I.), NNX10AI42G (D.S. Ebel, PI), NNX1OAG46G (H. Connolly, PI), NNX07AI46G, and NNX10AH77G (N. Kita, PI). WiscSIMS is partly supported by NSF (EAR03-19230, EAR05-16725, EAR07-44079).

REFERENCES

Andersen C. A., Keil K. and Mason B. (1964) Silicon oxynitride: a meteorite mineral. *Science* **146**, 256–257.

Brett R. and Sato M. (1984) Intrinsic oxygen fugacity measurements on seven chondrites, a pallasite, and tekitite and the redox state of meteorite parent bodies. *Geochim. Cosmochim. Acta* **48**, 111–120.

Chaussidon M., Libourel G. and Krot A. N. (2008) Oxygen isotopic constraints on the origin of magnesian chondrules and on the gaseous reservoir in the early solar system. *Geochim. Cosmochim. Acta* **72**, 1924–1938.

Ciesla F. J. (2007) Outward transport of high-temperature materials around the midplane of the solar nebula. *Science* **318**, 613–615.

Clayton R. N. and Mayeda T. K. (1984) Oxygen isotopic compositions of enstatite chondrites and aubrites. *J. Geophys. Res.* **89**, C245–C249.

Clayton R. N., Onuma N., Grossman L. and Mayeda T. K. (1977) Distribution of the presolar component in Allende and other carbonaceous chondrites. *Earth Planet. Sci. Lett.* **34**, 209–224.

Fagan T., McKeegan K. D., Krot A. N. and Keil K. (2001) Calcium–aluminum-rich inclusions in enstatite chondrites (II): oxygen isotopes. *Meteorit. Planet. Sci.* **36**, 223–230.

Grossman J. N., Rubin A. E., Rambaldi E. R., Rajan R. S. and Wasson J. T. (1985) Chondrules in the Qingzhen type-3 enstatite chondrite: possible precursor components and comparison to ordinary chondrite chondrules. *Geochim. Cosmochem. Acta* **49**, 1781–1795.

Guan Y., McKeegan K. D. and MacPherson G. J. (2000) Oxygen isotopes in calcium−aluminum-rich inclusions from enstatite chondrites: new evidence for a single CAI source in the solar nebula. *Earth Planet. Sci. Lett.* **181**, 271–277.

Ikeda Y. (1988) Petrolochemical study of the Yamato-691 enstatite chondrite (E3) I: major element chemical compositions of chondrules and inclusions. *Proc. NIPR Symp. Antarct. Meteor.* **1**, 3–13.

Ikeda Y. (1989) Petrolochemical study of the Yamato-691 enstatite chondrite (E3) III: descriptions and mineral compositions of chondrules. *Proc. NIPR Symp. Antarct. Meteor.* **2**, 75–108.

Javoy M. (1995) The integral enstatite chondrite model of the earth. *Geophys. Res. Lett.* **22**, 2219–2222.

Jones R. H. (1996) Relict grains in chondrules: evidence for chondrule recycling. In *Chondrules, the Protoplaneatry Disk* (eds. R. H. Hewins, R. H. Jones and E. R. D. Scott). Cambridge University Press, UK, pp. 163–172.

Jones R. H., Leshin L. A., Guan Y. B., Sharp Z. D., Durakiewicz T. and Schilk A. J. (2004) Oxygen isotope heterogeneity in chondrules from the Mokoia CV3 carbonaceous chondrite. *Geochim. Cosmochim. Acta* **68**, 3423–3438.

Keil K. (1968) Mineralogical and chemical relationships among enstatite chondrites. *J. Geophys. Res.* **73**, 6945–6976.

Keil K. and Andersen C. A. (1964) Electron microprobe study of the Jajh deh Kot Lalu enstatite chondrite. *Geochim. Cosmochim. Acta* **29**, 621–632.

Kimura M., Hiyagon H., Lin Y. and Weisberg M. K. (2003) FeO-rich silicate components in the Sahara 97159 (EH3) enstatite chondrite: their mineralogy, oxygen isotopic compositions and origin. *Meteorit. Planet. Sci.* **38**, 389–398.

Kita N. T., Ushikubo T., Kimura M., Nyquist L. E. and Valley J. W. (2008) Heterogeneous oxygen isotope ratios of olivine in chondrules from Y-793408 (H3.2) chondrite. *Meteorit. Planet. Sci. Suppl.* **43**, A77.

Kita N. T., Ushikubo T., Fu B. and Valley J. W. (2009) High precision SIMS oxygen isotope analysis and the effect of sample topography. *Chem. Geol.* **264**, 43–57.

Kita N. T., Nagahara H., Tachibana S., Tomomura S., spicuzza M. J., Founelle J. H. and Valley J. W. (2010) High precision SIMS oxygen three isotope study of chondrules in LL3 chondrites: role of ambient gas during chondrule formation. *Geochim. Cosmochim. Acta* **74**, 6610–6635.

Kunihiro T., Rubin A. E., McKeegan K. D. and Wasson J. T. (2004) Oxygen-isotopic compositions of relict and host grains in chondrules in the Yamato 81020 CO3.0 chondrite. *Geochim. Cosmochim. Acta* **68**, 3599–3606.

Kunihiro T., Rubin A. E. and Wasson J. T. (2005) Oxygen-isotopic compositions of low-FeO relicts in high-FeO host chondrules in Acfer 094, a type 3.0 carbonaceous chondrite closely related to CM. *Geochim. Cosmochim. Acta* **69**, 3831–3840.

Leitch C. A. and Smith J. V. (1982) Petrography, mineral chemistry and origin of Type I enstatite chondrites. *Geochim. Cosmochim. Acta* **46**, 2083–2097.

Lin Y., Kimura M., Hiyagon H. and Monoi A. (2003) Unusually abundant refractory inclusions from Sahara 97159 (EH3): a comparative study with other groups of chondrites. *Geochim. Cosmochim. Acta* **67**, 4935–4948.

Lusby D., Scott E. R. D. and Keil K. (1987) Ubiquitous high FeO silicates in enstatite chondrites. Proc. Lunar Planet. Sci. Conf. 17. *J. Geophys. Res. Suppl.* **92**, E679–E695.

Mason B. (1966) The enstatite chondrites. *Geochim. Cosmochim. Acta* **30**, 23–39.

Nagahara H. (1981) Evidence for secondary origin of chondrules. *Nature* **292**, 135–136.

Nagahara H. (1983) Chondrules formed through incomplete melting of pre-existing mineral clusters and the origin of chondrules. In *Chondrules and Their Origins* (ed. E. A. King). Lunar Planetary Institute, Houston., pp. 211–222.

Pouchou J. L. and Pichoir F. (1991) Quantitative analysis of homogeneous or stratified microvolumes applying the model "PAP". In *Electron Probe Quantitation* (eds. K. F. J. Heinrich and D. E. Newbury). Plenum Press, New York, NY, pp. 31–75.

Rambaldi E. R. (1981) Relict grains in chondrules. *Nature* **293**, 558–561.

Rambaldi E. R., Rajan R. S., Wang D. and Housley R. M. (1983) Evidence for relict grains in chondrules of Qingzhen, an E3 type enstatite chondrite. *Earth Planet. Sci. Lett.* **66**, 11–24.

Russell S. S., MacPherson G. J., Leshin L. A. and Mckeegan K. D. (2000) O-16 enrichments in aluminum-rich chondrules from ordinary chondrites. *Earth Planet. Sci. Lett.* **184**, 57–74.

Schneider D. M., Symes S. J. K., Benoit P. H. and Sears D. W. G. (2002) Properties of chondrules in EL3 chondrites, comparison with EH3 chondrites, and implications for the formation of enstatite chondrites. *Meteorit. Planet. Sci.* **37**, 1401–1416.

Shu F. H., Najita J., Ostriker E. C. and Shang H. (1995) Magnetocentrifugally driven flows from young stars and disks. V. Asymptotic collimation into jets. *Astrophys. J. Lett.* **455**, L155–L158.

Ushikubo T., Kimura M., Kita, N. T. and Valley J. W. (2011) Primordial oxygen isotope reservoirs of the solar nebula recorded in chondrules from Acfer 094 carbonaceous chondrite. *Lunar Planet. Sci. XLII.*, #1183 (abstr.).

Weisberg M. K., Bosenberg J. S., Kozhusko G., Prinz M., Clayton R. N. and Mayeda T. K. (1995) EH3 and EL3 chondrites: a petrologic-oxygen isotopic study. *Lunar Planet. Sci.* **XXVI**, 1481–1482.

Weisberg M. K., Prinz M. and Fogel R. A. (1994) The evolution of enstatite and chondrules in unequilibrated enstatite chondrites: evidence from iron-rich pyroxene. *Meteoritics* **29**, 362–373.

Weisberg M. K., Kimura M., McCoy T. J. and Lin Y. (2005) Olivine and the thermal history of the E chondrite parent body. *Lunar Planet Sci. XXXVI.*, # 1420 (abstr.).

Yurimoto H. and Kuramoto K. (2004) Molecular cloud origin for oxygen isotope heterogeneity in the solar system. *Science* **305**, 1763–1766.

Yurimoto H. and Wasson J. T. (2002) Extremely rapid cooling of a carbonaceous-chondrite chondrule containing very ^{16}O-rich olivine and a ^{26}Mg-excess. *Geochim. Cosmochim. Acta* **66**, 4355–4363.

Associate editor: Alexander N. Krot